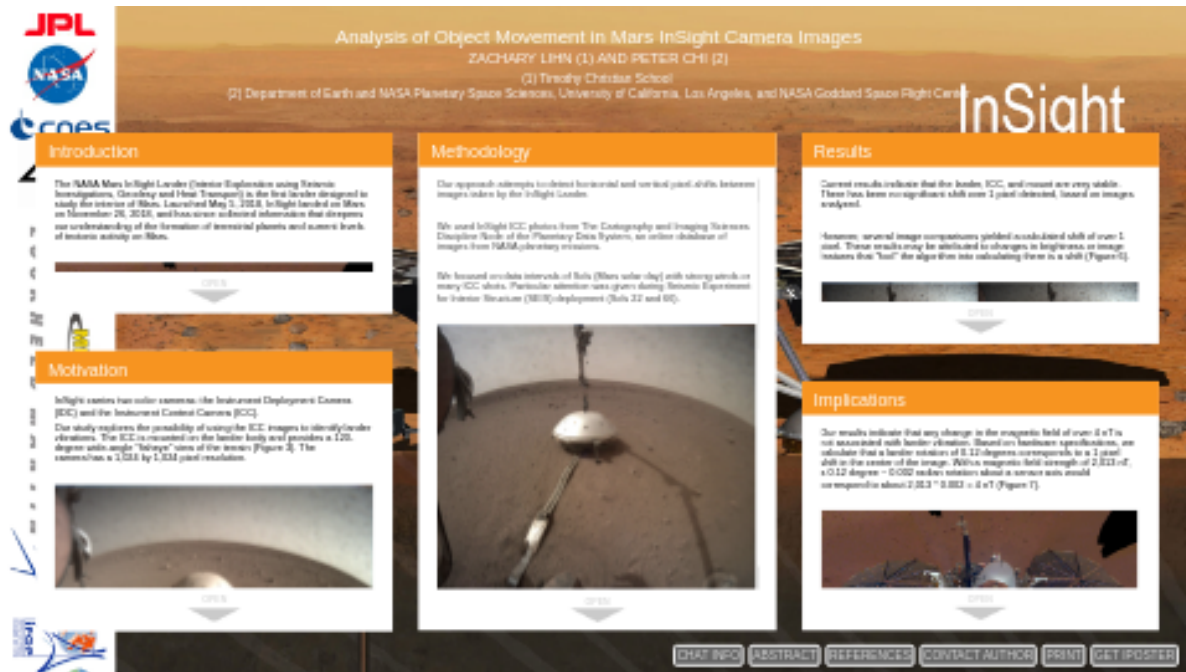


Analysis of Object Movement in Mars InSight Camera Images

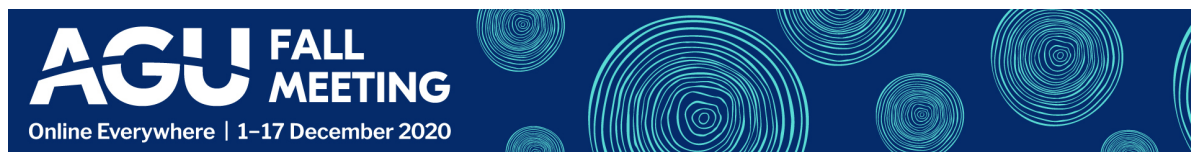


ZACHARY LIHN (1) AND PETER CHI (2)

(1) Timothy Christian School

(2) Department of Earth and NASA Planetary Space Sciences, University of California, Los Angeles, and NASA Goddard Space Flight Center

PRESENTED AT:



INTRODUCTION

The NASA Mars InSight Lander (Interior Exploration using Seismic Investigations, Geodesy and Heat Transport) is the first lander designed to study the interior of Mars. Launched May 5, 2018, InSight landed on Mars on November 26, 2018, and has since collected information that deepens our understanding of the formation of terrestrial planets and current levels of tectonic activity on Mars.

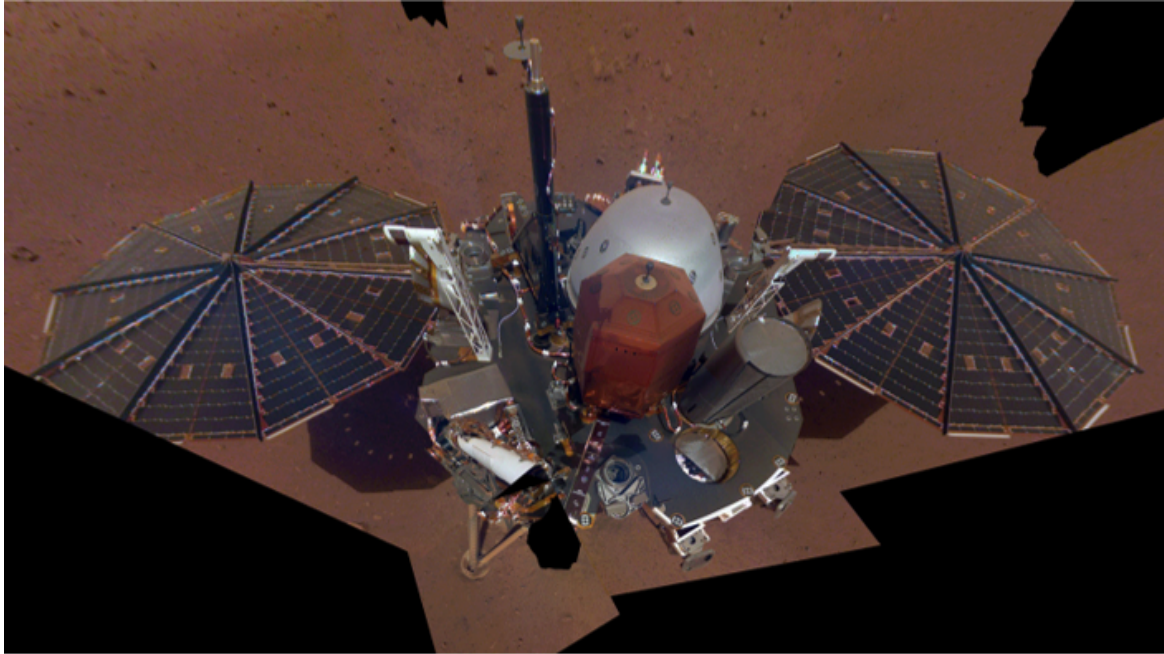


Figure 1. Composite photo of the InSight Lander.

Mars is an optimal choice for the study of early history in terrestrial planets. Due to Mars' smaller size compared to Earth and its lack of tectonic plates, information about Mars' geological history has been preserved in its natural structure. For example, the constant motion and churning of Earth's tectonic plates have erased structural evidence of its early history in the crust and mantle. Meanwhile, Mars' mantle and crust are relatively intact. They can provide insight into the early evolution of other rocky planets such as Earth and Mars.

Using the seismometer (SEIS), Heat Flow and Physical Properties Package (HP3), flux magnetometer (IFG), and other sensitive instruments (Figure 2), the lander records data about Mars' seismic activity, heat flow, magnetic field, and more.

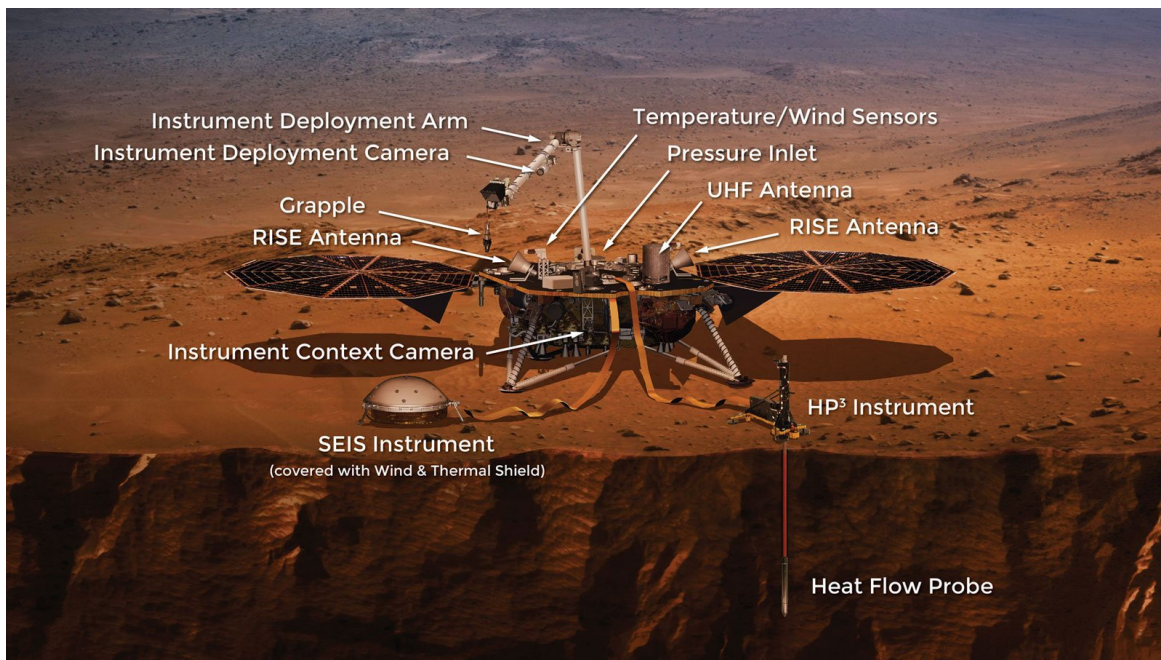


Figure 2. Location of InSight instruments. Note the placement of the Instrument Context Camera (ICC).

MOTIVATION

InSight carries two color cameras: the Instrument Deployment Camera (IDC) and the Instrument Context Camera (ICC).

Our study explores the possibility of using the ICC images to identify lander vibrations. The ICC is mounted on the lander body and provides a 120-degree wide-angle "fisheye" view of the terrain (Figure 3). The camera has a 1,024 by 1,024 pixel resolution.

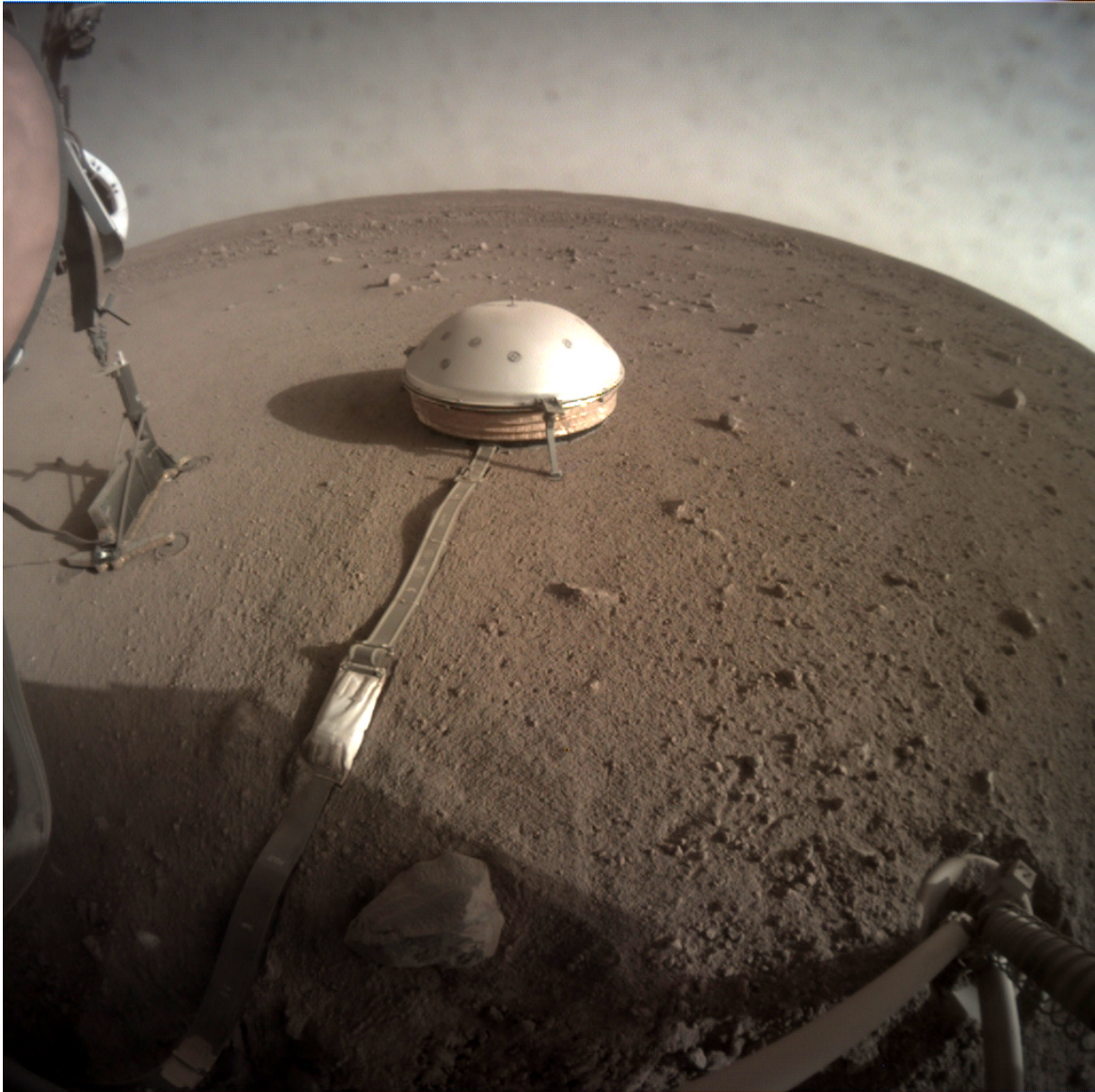


Figure 3. ICC photo taken on Sol 202.

The strong magnetic field at the landing site was a surprise (2,013 nT). Magnetic field strength was 10 times stronger than expected compared to satellite predictions prior to landing (Johnson et al. 2020).

By detecting lander vibrations, we attempt to infer the background magnetic field. We test if the magnetic field displaces or rotates the lander by comparing pixel differences between images.

METHODOLOGY

Our approach attempts to detect horizontal and vertical pixel-shifts between images taken by the InSight Lander.

We used InSight ICC photos from The Cartography and Imaging Sciences Discipline Node of the Planetary Data System, an online database of images from NASA planetary missions.

We focused on data intervals of Sols (Mars solar day) with strong winds or many ICC shots. Particular attention was given during Seismic Experiment for Interior Structure (SEIS) deployment (Sols 22 and 66).

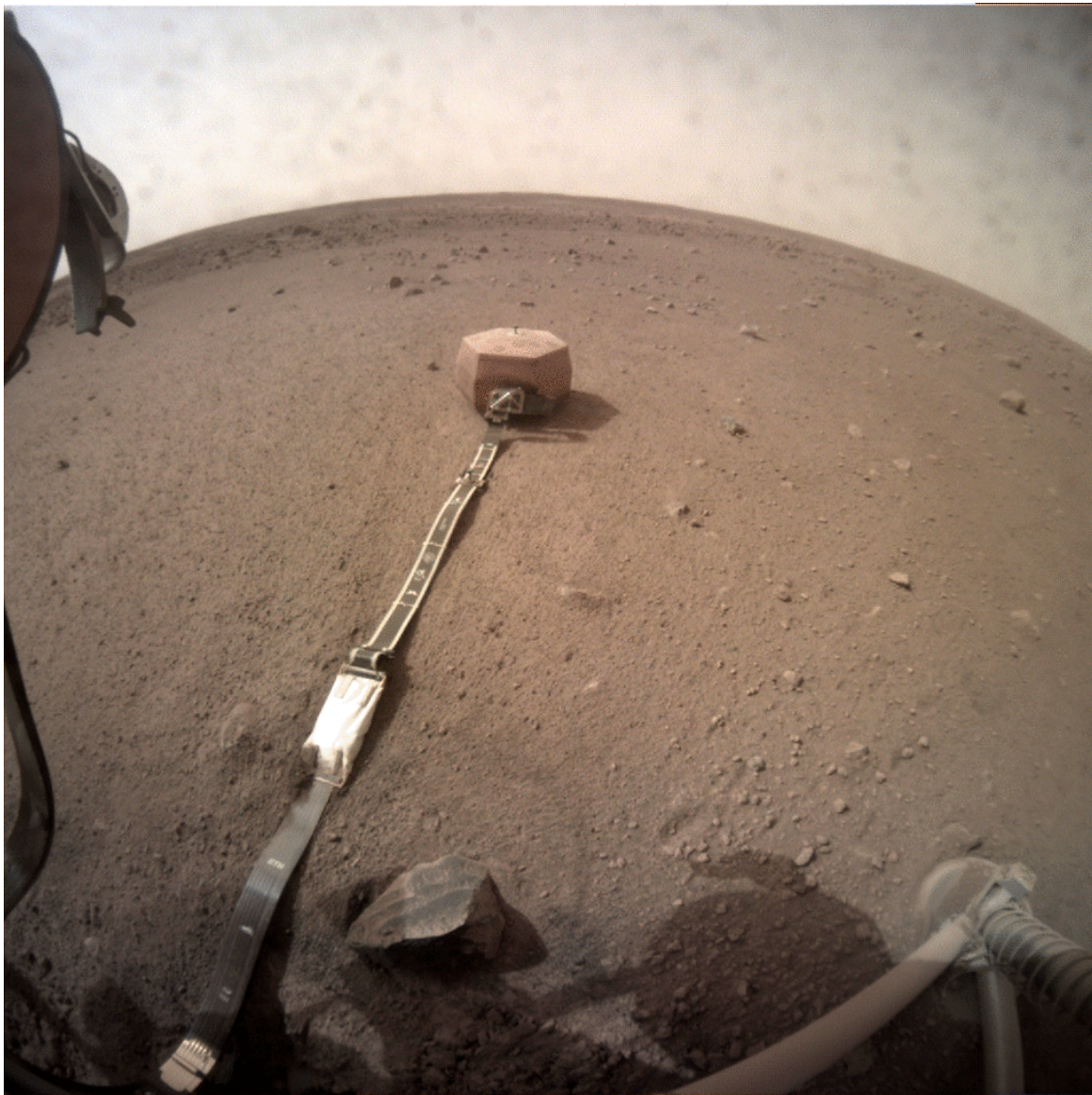


Figure 4. Deployment of SEIS cover on Sol 66.

Using a Java program, we converted ICC EDR images to grayscale. The grayscale conversion was done with the equation $0.299 \cdot \text{Red} + 0.587 \cdot \text{Green} + 0.114 \cdot \text{Blue}$.

For each pair of images, we found the horizontal and vertical pixel-shifts that minimize

$$\sum(\Delta I)^2$$

where

$$\Delta I$$

is the difference in intensity between two images. The sum is taken over all pixels in the image. A pairwise comparison was performed on over 150 images.

We assume there is no loose mount of the ICC or IFG on the lander.

A caveat is that the method is useful when the lander rotates rather than displaces (Figure 5). If the magnetic field is uniform and the lander shifts horizontally with no rotations, the lander will not detect any changes in magnetic field measurements.

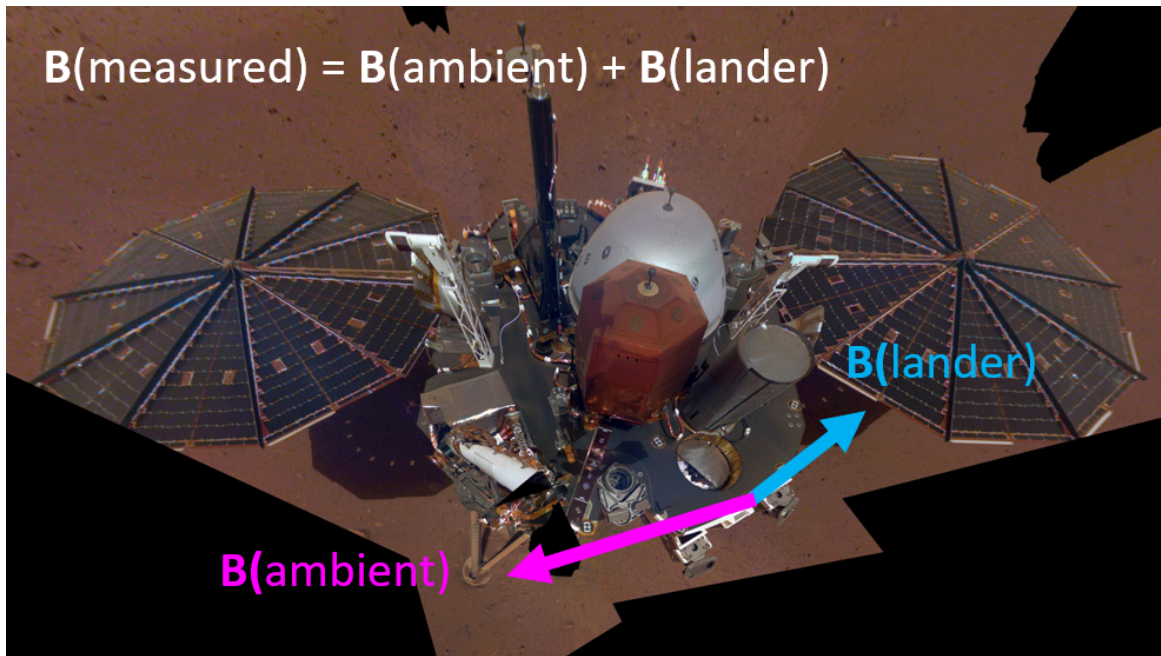


Figure 5. If the field is uniform, lander displacement in a lateral direction will not affect magnetic field measurement, that is, $B(\text{lander}) = 0$. However, if $B(\text{ambient})$ and $B(\text{lander})$ are not parallel, $B(\text{lander})$ will not be 0 and the lander will detect a change in the magnetic field.

RESULTS

Current results indicate that the lander, ICC, and mount are very stable. There has been no significant shift over 1 pixel detected, based on images analyzed.

However, several image comparisons yielded a calculated shift of over 1 pixel. These results may be attributed to changes in brightness or image features that "fool" the algorithm into calculating there is a shift (Figure 6).

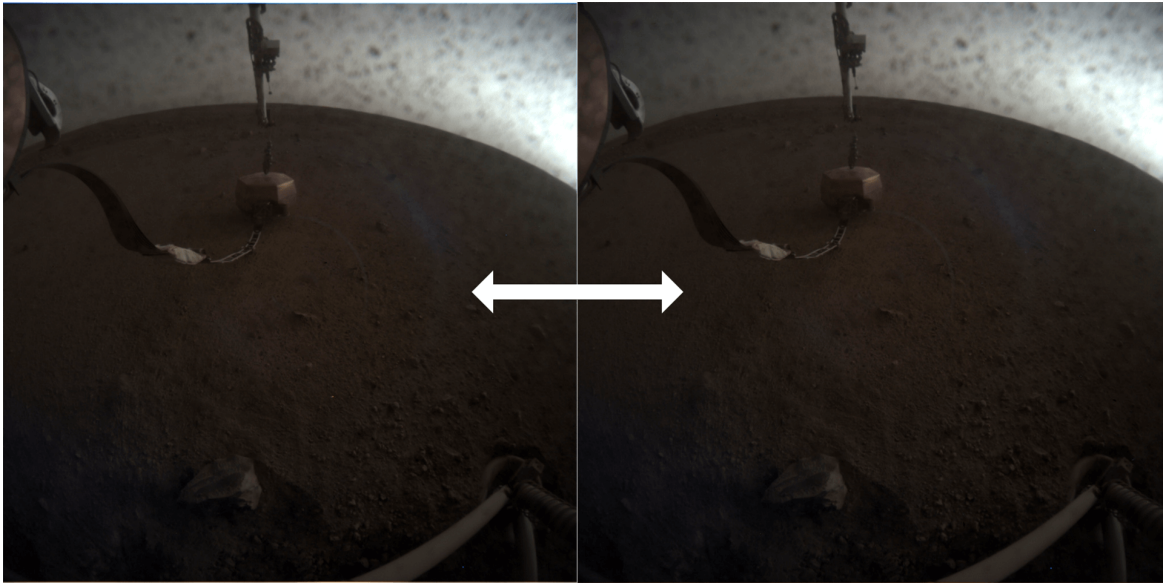


Figure 6. Two images with a calculated shift of over 40 pixels. Notice the darkness and dirt on the camera lens. We assert that the real image shift cannot be inferred from the algorithm. The changes in the subject of the photos, rather than perspective, create differences in pixel intensity that lead to false positives in the code.

IMPLICATIONS

Our results indicate that any change in the magnetic field of over 4 nT is not associated with lander vibration. Based on hardware specifications, we calculate that a lander rotation of 0.12 degrees corresponds to a 1 pixel shift in the center of the image. With a magnetic field strength of 2,013 nT, a 0.12 degree ~ 0.002 radian rotation about a sensor axis would correspond to about $2,013 * 0.002 = 4$ nT (Figure 7).

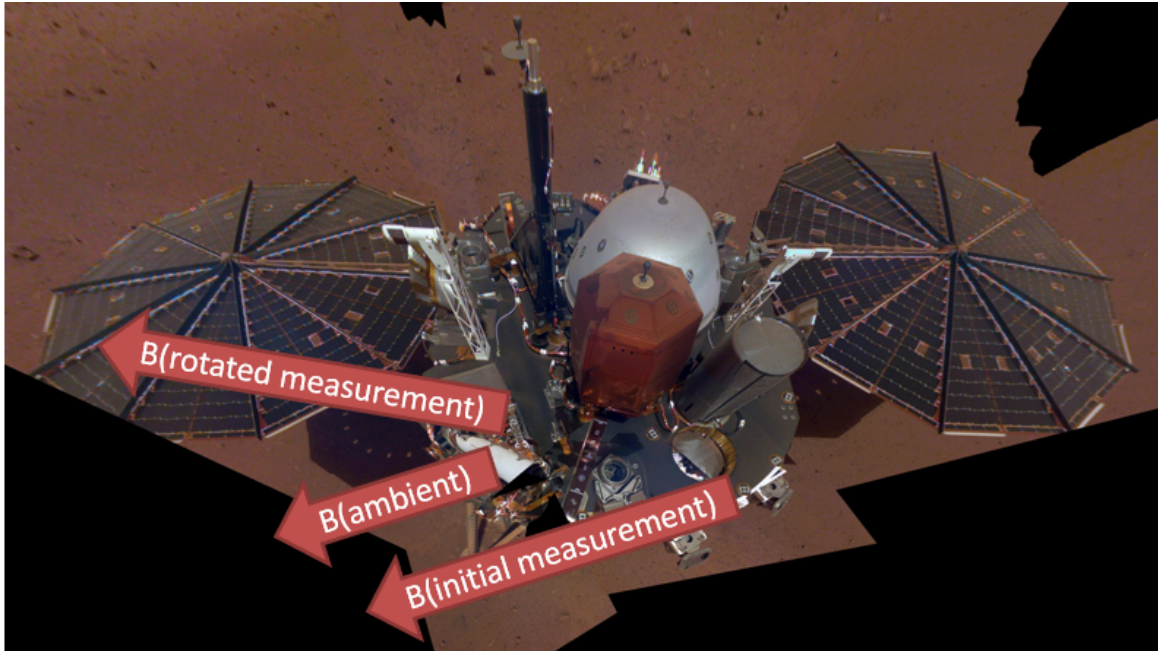


Figure 7. Suppose the background magnetic field and magnetic sensor are aligned in the x-direction. Then $B(\text{ambient}) = (2013, 0, 0)$ and $B(\text{initial measurement}) = (2013, 0, 0)$. If there is a rotation of 0.002 radians spanning in the direction of the y-axis, then the sensor reading, $B(\text{rotated measurement})$, will change. The y-component of this new vector becomes 4 nT.

Since we have not detected image shifts of over 1 pixel, we conclude that changes in the magnetic field of over 4 nT do not rotate the lander.

In future results, we plan to refine our analysis by examining a larger data set. We will also focus on more specific portions of photos, such as edges or areas of high contrast. This would eliminate false positives, as in Figure 6.

Our image analysis method may also be applied to other images on the InSight lander. We may use IDC photos to examine deck activity and the HP³ mole.

ABSTRACT

The NASA Mars InSight lander carries two color cameras: The Instrument Context Camera (ICC), a wide-angle camera mounted to the lander, and the Instrument Deployment Camera (IDC), mounted to the lander robotic arm. The cameras provide both valuable information for lander and instrument operation and essential data for a range of scientific studies. In this study, we examine ICC images to investigate whether there is any shift that might be associated with lander movement. Detection of lander movement may lead to potential applications, including a possibility of inferring the background magnetic field. We focused on the data intervals where there were strong winds, many ICC images taken during the Martian day, or during seismometer deployment. Because any potential shift in ICC images is expected to be minuscule, we developed a computer program to search for the shift between images which minimizes the sum of squared differences in brightness. The preliminary results indicate that the lander, ICC, and the mount are very robust. Our image analysis method is suitable for identifying object movement in color images from both InSight cameras.

REFERENCES

Johnson, C.L., Mittelholz, A., Langlais, B. et al. Crustal and time-varying magnetic fields at the InSight landing site on Mars. *Nat. Geosci.* 13, 199–204 (2020). <https://doi.org/10.1038/s41561-020-0537-x>

Figure 1. *InSight's First Selfie*, 2018, Jet Propulsion Laboratory. Retrieved from <https://www.jpl.nasa.gov/spaceimages/details.php?id=PIA22876> (<https://www.jpl.nasa.gov/spaceimages/details.php?id=PIA22876>).

Figure 2. *Artist's Concept of InSight Lander on Mars*, 2018, NASA Mars InSight Mission. Retrieved from <https://mars.nasa.gov/insight/spacecraft/instruments/summary/> (<https://mars.nasa.gov/insight/spacecraft/instruments/summary/>).

Figure 3. PDS Imaging Node. Retrieved from https://pds-imaging.jpl.nasa.gov/data/nsyt/insight_cameras/.

Figure 4. PDS Imaging Node. Retrieved from https://pds-imaging.jpl.nasa.gov/data/nsyt/insight_cameras/. GIF compiled by Zachary Lihn.

Figure 5. *InSight's First Selfie*, 2018, Jet Propulsion Laboratory. Retrieved from <https://www.jpl.nasa.gov/spaceimages/details.php?id=PIA22876> (<https://www.jpl.nasa.gov/spaceimages/details.php?id=PIA22876>). Symbols and text overlay added by Dr. Peter Chi.

Figure 6. PDS Imaging Node. Retrieved from https://pds-imaging.jpl.nasa.gov/data/nsyt/insight_cameras/. Symbols added by Zachary Lihn.

Figure 7. PDS Imaging Node. Retrieved from https://pds-imaging.jpl.nasa.gov/data/nsyt/insight_cameras/. Symbols and text added by Zachary Lihn.